



^{238}U - ^{230}Th dating of chevkinite in high-silica rhyolites from La Primavera and Yellowstone calderas

Jorge A. Vazquez ^{a,*}, Noel O. Velasco ^b, Axel K. Schmitt ^c, Heather A. Bleick ^a, Mark E. Stelten ^d

^a United States Geological Survey, 345 Middlefield Road, Mail Stop 910, Menlo Park, CA 94028, USA

^b Department of Geological Sciences, California State University—Northridge, 18111 Nordhoff Street, Los Angeles, CA 91330, USA

^c Department of Earth, Planetary, and Space Sciences, University of California—Los Angeles, 595 Charles Young Drive East, Los Angeles, CA 90095, USA

^d Department of Geology, University of California—Davis, One Shields Avenue, Davis, CA 95616, USA



ARTICLE INFO

Article history:

Received 24 July 2014

Received in revised form 14 October 2014

Accepted 21 October 2014

Available online 29 October 2014

Editor: K. Mezger

Keywords:

Chevkinite

Uranium-series geochronology

Ion microprobe

Yellowstone

La Primavera

Rhyolite

ABSTRACT

Application of ^{238}U - ^{230}Th disequilibrium dating of accessory minerals with contrasting stabilities and compositions can provide a unique perspective on magmatic evolution by placing the thermochemical evolution of magma within the framework of absolute time. Chevkinite, a Th-rich accessory mineral that occurs in peralkaline and metaluminous rhyolites, may be particularly useful as a chronometer of crystallization and differentiation because its composition may reflect the chemical changes of its host melt. Ion microprobe ^{238}U - ^{230}Th dating of single chevkinite microphenocrysts from pre- and post-caldera La Primavera, Mexico, rhyolites yields model crystallization ages that are within 10's of k.y. of their corresponding K-Ar ages of ca. 125 ka to 85 ka, while chevkinite microphenocrysts from a post-caldera Yellowstone, USA, rhyolite yield a range of ages from ca. 110 ka to 250 ka, which is indistinguishable from the age distribution of coexisting zircon. Internal chevkinite-zircon isochrons from La Primavera yield Pleistocene ages with ~5% precision due to the nearly two order difference in Th/U between both minerals. Coupling chevkinite ^{238}U - ^{230}Th ages and compositional analyses reveals a secular trend of Th/U and rare earth elements recorded in Yellowstone rhyolite, likely reflecting progressive compositional evolution of host magma. The relatively short timescale between chevkinite-zircon crystallization and eruption suggests that crystal-poor rhyolites at La Primavera were erupted shortly after differentiation and/or reheating. These results indicate that ^{238}U - ^{230}Th dating of chevkinite via ion microprobe analysis may be used to date crystallization and chemical evolution of silicic magmas.

Published by Elsevier B.V.

1. Introduction

High-resolution ^{238}U - ^{230}Th dating of accessory minerals with contrasting stabilities and compositions (e.g., allanite and zircon) can provide a unique perspective on magmatic evolution by placing the thermochemical changes of silicic magma within a framework of absolute time. Chevkinite-(Ce), a titanosilicate $[\text{Ce}_4(\text{Ti}, \text{Fe}^{2+}, \text{Fe}^{3+})_5\text{O}_8(\text{Si}_2\text{O}_7)_2]$ that typically has elevated Th concentrations and occurs in peralkaline and metaluminous rhyolites as microphenocrysts and inclusions in major phases, may be particularly useful as a chronometer of crystallization and differentiation in magma chambers because its composition may reflect the chemical changes of its host melt and it is amenable to ^{238}U - ^{230}Th geochronology. Magma reservoirs associated with calderas that erupt the largest volumes of silicic magma assemble and evolve over timescales of 10^3 to 10^5 years (Costa, 2008; Gelman et al., 2013). Hence, the ^{238}U - ^{230}Th system with its ability to date crystallization ages over 10^3 - 10^4 year intervals is optimized for resolving the crystallization

history of magmas at young calderas (see reviews by Cooper and Reid, 2008; Schmitt, 2011). Pioneering studies using ^{238}U - ^{230}Th disequilibrium to date crystallization of accessory minerals employed multi-grain analysis (e.g., Fukuoka and Kigoshi, 1974; Pyle et al., 1988) with unavoidable uncertainty about the age variation between and within single crystals. The advent of ion microprobe ^{238}U - ^{230}Th geochronology greatly reduced this uncertainty by dating domains within single crystals, allowing unique insight into the timing of accessory mineral crystallization relative to eruption (e.g., Reid et al., 1997), intra-crystal age distribution (e.g., Storm et al., 2011), crystal growth rates (e.g., Schmitt et al., 2011) and the magnitudes of inheritance and antecrustic recycling (e.g., Bacon and Lowenstern, 2005).

This paper describes ion microprobe ^{238}U - ^{230}Th dating of chevkinite from Pleistocene rhyolites erupted from La Primavera and Yellowstone calderas (Fig. 1), both of which have protracted volcanic histories that are delimited by K-Ar and ^{40}Ar / ^{39}Ar geochronology. Chevkinite microphenocrysts from pre- and post-caldera lavas from La Primavera yield model ^{238}U - ^{230}Th crystallization ages that are consistent with crystallization ages for coexisting zircon, and which match or are within 10's of k.y. of their corresponding K-Ar ages of ca. 125 ka and ca. 85 ka. When combined, associated chevkinite and zircon crystals yield isochron ages

* Corresponding author. Tel.: +1 650 329 5240.

E-mail addresses: jvazquez@usgs.gov (J.A. Vazquez), axelk@argon.ess.ucla.edu (A.K. Schmitt), hbleick@usgs.gov (H.A. Bleick), mestelten@ucdavis.edu (M.E. Stelten).

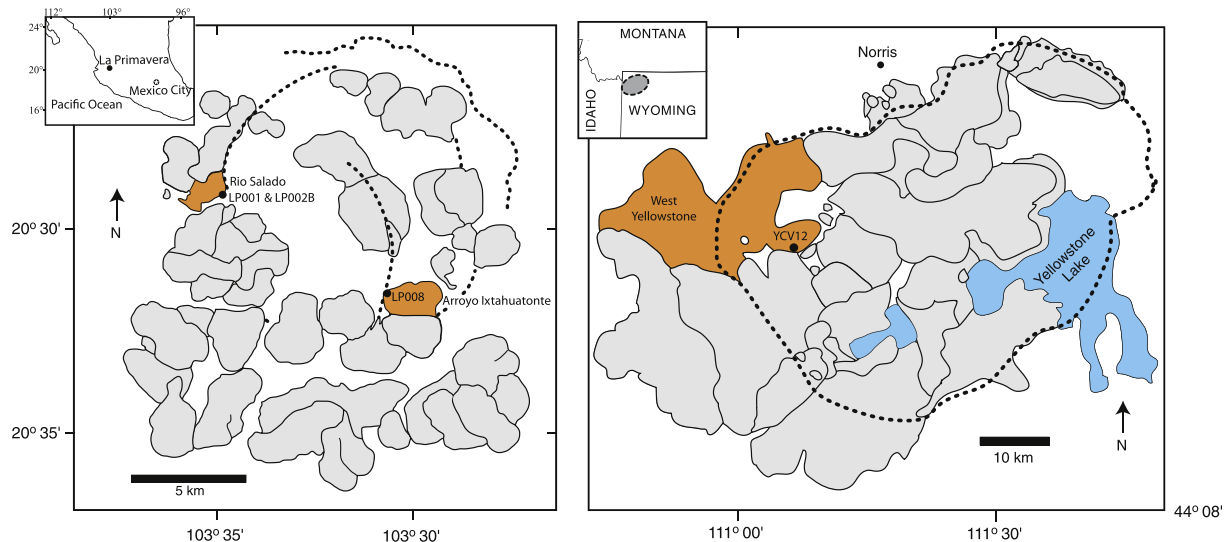


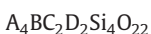
Fig. 1. Locations of La Primavera and Yellowstone calderas with individual post-caldera lava flows outlined as gray fields. Sampled rhyolite lavas are plotted in orange. Dashed lines are caldera faults. Maps after Mahood (1981) and Christiansen (2001).

with ~5% precision due to the nearly two order difference in Th/U between both minerals. Chevkinite microphenocrysts from the post-caldera West Yellowstone flow at Yellowstone caldera yield model ages that range up to approximately 200 k.y. before their $^{40}\text{Ar}/^{39}\text{Ar}$ eruption age of ca. 115 ka, and that match the range of crystallization ages recorded by coexisting zircon. When keyed to composition, the chevkinite ages reveal secular variation of crystal composition that is likely to reflect the compositional evolution of host magma. These results demonstrate that ion microprobe U-Th dating of single chevkinite crystals may resolve the time-compositional chronology for differentiation of rhyolitic magma.

1.1. Compositions and crystallization of chevkinite-(Ce) in silicic magmas

Chevkinite occurs as microphenocrysts or inclusions in major phases in a range of evolved silicic volcanic rocks including trachyte and comendite (e.g., Cameron and Cameron, 1986; Novak and Mahood, 1986; Michael, 1988; Scaillet and Macdonald, 2001; Macdonald et al., 2002; Heumann and Davies, 2002; Troll et al., 2003; Johnson et al., 1989) as well as evolved “A-type” rhyolites (e.g. Young and Powers, 1960; Izett and Wilcox, 1968; Johnson et al., 1989; Mills et al., 1997; Macdonald and Belkin, 2002; Min et al., 2006; Cubukcu et al., 2007). Plutonic equivalents such as syenites and granitoids from a variety of tectonic settings may also contain chevkinite (e.g., Lowenstein et al., 1997; Robinson and Miller, 1999; Verplanck et al., 1999; Schmitt et al., 2000; Ridolfi et al., 2003; Bacon et al., 2007; Vlach and Gualda, 2007).

Chevkinite in silicic volcanic rocks may contain several weight (wt.) % ThO_2 with Th/U ratios up to ~60 (Macdonald et al., 2002, 2009). Like allanite, the high concentration of Th and a large excess of ^{230}Th relative to ^{238}U during crystallization make young chevkinite ideal for ^{238}U - ^{230}Th disequilibrium dating. In chevkinite, quadrivalent Th and U are accommodated in the A-site site according to the general formula:



where A = rare earth element (REE), Ca, Th, U; B = Fe^{2+} ; C = Ti, Al, Zr, Nb, Mg, Mn, Fe^{3+} , Fe^{2+} and D = Ti (Macdonald and Belkin, 2002), with the most abundant REE being La, Ce, Pr, Nd, and Sm. In chevkinite, charge balancing for REE incorporation follows:

$$(\text{Ca}^{2+})_A + (\text{Ti}^{4+})_C = [(\text{REE}, \text{Y})^{3+}]_A + (\text{M}^{2+,3+})_C$$

(McDowell, 1979; Green and Pearson, 1988) and:

$$(\text{Ca}^{2+})_A + (\text{Ti}^{4+})_C + (\text{Zr}^{4+})_C = [(\text{REE}, \text{Y})^{3+}]_A + (\text{M}^{2+,3+})_C$$

(Vlach and Gualda, 2007) where REE = rare earth elements, A = A site, C = C site, and M_C = Fe, Al, Mg, Zr, Nb, P, and K (McDowell, 1979; Macdonald and Belkin, 2002). Concentrations of light rare earth elements (LREEs) typically range between 9–25 wt.% $(\text{Ce}, \text{La})_2\text{O}_3$ (Macdonald et al., 2002, 2009), giving chevkinite some of the highest observed crystal/melt partition coefficients for LREE (Macdonald et al., 2002; Troll et al., 2003). Heavy rare earth element concentrations in chevkinite are typically 1–3 orders of magnitude lower than LREE (Macdonald et al., 2002). Hence, crystallization and fractionation of chevkinite may be apparent from LREE concentration trends in suites of silicic magmas related by fractional crystallization even if crystals are a small minority of the crystal mode (e.g., Cameron and Cameron, 1986; Parker and White, 2007). Variation in the composition of igneous chevkinite may reflect magmatic evolution, with distinctions between phenocryst and groundmass crystals of plutonic rocks (McDowell, 1979) and in some cases within single crystals (Macdonald and Belkin, 2002; Vlach and Gualda, 2007).

The solubility of chevkinite in peralkaline and metaluminous silicic magma is not yet established by a comprehensive set of experiments. The importance of temperature, magma composition, oxygen fugacity, and concentrations of essential structural constituents, in this case LREE and Ti concentrations, in host melt are underscored by phase-equilibrium experiments on peralkaline rhyolites from East Africa (Scaillet and Macdonald, 2003) and REE-doped silicic compositions (Green and Pearson, 1988), as well as theoretical considerations (Bacon, 1989) and observed suites of rocks (e.g., Vlach and Gualda, 2007). Crystallization of chevkinite in metaluminous magma appears to occur at a more restricted temperature range than for crystallization in peralkaline magmas. Chevkinite-bearing metaluminous rhyolites typically yield crystallization temperatures that are >760 °C (e.g., Izett and Wilcox, 1968; Vazquez et al., 2009). At lower temperatures, allanite is the stable LREE-rich phase (e.g., Hildreth et al., 1984). In contrast, peralkaline silicic magmas containing chevkinite yield Fe-Ti oxide and two-pyroxene temperatures between ~700 °C and ~1000 °C (e.g., Novak and Mahood, 1986; Scaillet and Macdonald, 2003; Troll et al., 2003).

1.2. Chevkinite in La Primavera and Yellowstone rhyolites

Chevkinite-bearing rhyolites have erupted from La Primavera, Mexico, and Yellowstone, USA, calderas (Fig. 1). La Primavera is a Quaternary caldera located next to Guadalajara, Jalisco, Mexico, along the western segment of the Trans-Mexican volcanic arc (Fig. 1). Multiple eruptions of porphyritic to aphyric high-silica rhyolite between ca. 140 and 30 ka generated a series of rhyolitic domes and coulees that are exposed over an ~500 km² area (Mahood, 1980; Walker et al., 1981). This volcanism was punctuated by the explosive eruption of ~40 km³ of rhyolite at ca. 95 ka, generating La Primavera caldera and the compositionally zoned Tala Tuff ignimbrite (Mahood, 1981; Mahood and Drake, 1982). La Primavera rhyolites contain <<1% modal chevkinite (Michael, 1988) that occurs as microphenocrysts in groundmass glass, typically associated with clusters of clinopyroxene, fayalite, zircon, and Fe-Ti oxides, and inclusions in major phases (Fig. 2).

Voluminous high-silica rhyolites characterize silicic volcanism associated with the Yellowstone hotspot. At Yellowstone caldera, multiple episodes of intracaldera volcanism have occurred since explosive eruption of the Lava Creek Tuff and caldera formation at ca. 640 ka (Christiansen, 2001; Lanphere et al., 2002). The youngest episode of caldera volcanism erupted more than 600 km³ of rhyolite, primarily as lava, between ca. 170 ka and ca. 75 ka (Christiansen et al., 2007). These rhyolites compose the Central Plateau Member (CPM) of the Plateau Rhyolite and cover much of the caldera floor (Christiansen and Blank, 1972; Christiansen, 2001). Age-correlated changes in the trace element and isotopic composition of CPM glasses and minerals, as well as geothermometry, suggest open-system evolution of a cooling magma reservoir that was periodically replenished with new rhyolite (Vazquez et al., 2009; Watts et al., 2012; Stelten et al., 2013).

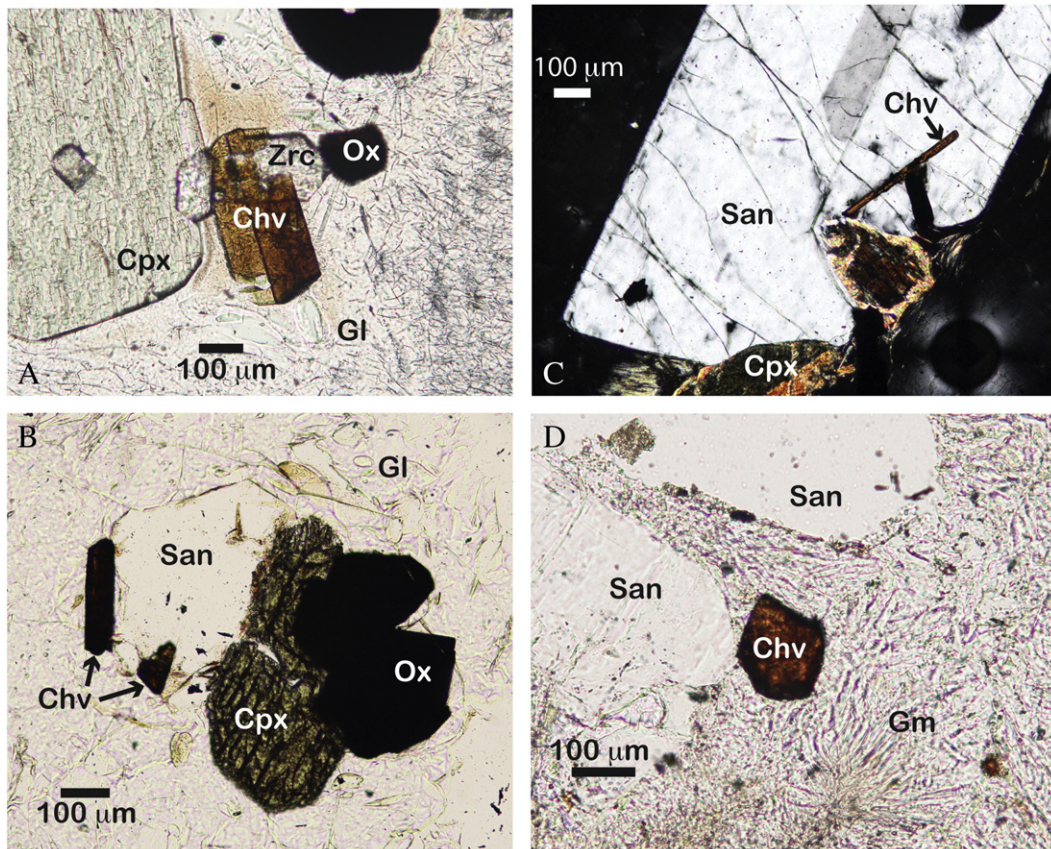


Fig. 2. Chevkinite microphenocrysts in high-silica rhyolite from Yellowstone and La Primavera calderas. A: Plane-polarized light (PPL) photomicrograph of Yellowstone chevkinite (Chv) intergrown with zircon (Zrc), titanomagnetite (Ox) and ferrohedenbergite (Cpx) in glass (Gl) groundmass. B: PPL image of La Primavera chevkinite and sanidine (San) in glassy Rio Salado rhyolite. C: Cross-polarized light image of chevkinite inclusion in Arroyo Ixtahuatonte sanidine. D: Rio Salado chevkinite with sanidine and ferrohedenbergite in devitrified groundmass (Gm).

In Yellowstone rhyolites, chevkinite occurs as microphenocrysts in groundmass glass and inclusions in clinopyroxene and fayalite, and like La Primavera chevkinite it is typically associated with clusters of mafic oxide and silicate phenocrysts (Fig. 2).

2. Samples and analytical methods

Using standard heavy liquid techniques, chevkinite and zircon were separated from two samples of ca. 125 ka precaldera Rio Salado dome and one hand sample of the ca. 85 ka postcaldera Arroyo Ixtahuatonte dome at La Primavera caldera (Fig. 1). Single chevkinite crystals were separated from the ca. 115 ka West Yellowstone flow at Yellowstone caldera. These West Yellowstone flow chevkinite crystals are from the same sample used by Vazquez and Reid (2002) for ²³⁸U–²³⁰Th ion microprobe dating of zircon. Individual crystals of chevkinite and zircon were cast in epoxy and indium mounts for ion and electron microprobe analysis. The smallest (<100 µm) chevkinite and zircon crystals were embedded in indium metal in order to prevent the generation of ²³²Th¹⁶O¹²C²⁺ when the primary ion beam partly overlaps onto epoxy surrounding a Th-bearing matrix and interferes with ²³⁰Th¹⁶O⁺ (Schmitt et al., 2006). The positive mass defect of ²³⁰Th and high mass resolution analysis ensures that any ¹¹⁵In¹⁶O⁺ derived from primary beam overlap of the surrounding indium is well resolved from ²³⁰Th¹⁶O⁺. Prior to analysis, mounts were washed in soapy water and finally rinsed with dilute HCl acid. The mounts were coated with a thin (~10 nm) layer of gold to create a conducting surface for ion microprobe analysis.

Ion microprobe analyses of chevkinite and zircon were performed with the Stanford-USGS SHRIMP-RG and UCLA CAMECA ims 1270 high-resolution ion microprobes. For SHRIMP-RG analyses, chevkinite was analyzed with a 12–18 nA ¹⁶O₂⁺ primary beam with 10 kV acceleration

focused to an ~40 μm diameter spot on sample surfaces. For CAMECA ims 1270 analyses, chevkinite and zircon were analyzed with a 20–80 nA $^{16}\text{O}^-$ primary beam with 12.5 kV acceleration and focused to an ~40 μm diameter spot. Samples were pre-sputtered for 10 to 60 s before the start of each analysis. Positive secondary ions were extracted and accelerated into the mass analyzers at 10 kV potential and measured at mass resolutions ($m/\Delta m$ at 10% peak height) of ~4500 (ims 1270) and ~9000 (SHRIMP-RG). Peak hopping using a single electron multiplier was employed for all chevkinite analyses except for one session (ims 1270) during which measurements were performed by static multi-collection using a Faraday cup for $^{232}\text{Th}^{16}\text{O}^+$ and electron multipliers for other masses. Cross-calibration of collectors during multi-collection was performed using measured versus the natural $^{238}\text{U}/^{235}\text{U}$ ratios. Secondary ions of $^{230}\text{Th}^{16}\text{O}^+$, $^{232}\text{Th}^{16}\text{O}^+$, and $^{238}\text{U}^{16}\text{O}^+$ were used for age calculations instead of their corresponding metal species because oxide secondary ion yields for chevkinite are 8–10 times greater than for their corresponding metals. Centering of the $^{230}\text{Th}^{16}\text{O}^+$ peak was guided using a persistent $^{150}\text{Nd}^{48}\text{Ti}^{16}\text{O}_3^+$ peak that is surrounded by overlapping LREE–Fe–Si–O peaks in the 245.8 atomic mass/charge region (Fig. 3). Analyses of La Primavera zircon were performed using the ims 1270 in multicollection mode following conditions described in Wetzel et al. (2010). Reported ratios are corrected for deadtime and background.

Relative sensitivity factors (RSFs) to account for differential ionization of ThO^+ and UO^+ were determined by repeated measurement of $^{230}\text{Th}^{16}\text{O}^+/\text{U}^{16}\text{O}^+$ in fragments from a single crystal of non-metamict chevkinite from a Pakistani pegmatite (Liziero, 2008) assumed to be in secular equilibrium ($^{230}\text{Th}/^{238}\text{U} = 1.694 \times 10^{-5}$). This chevkinite ("Arondu") contains 0.8–2.2 wt.% ThO_2 based on electron microprobe analyses (Appendix A) with apparent U concentrations of up to 1900 ppm. Similar to allanite (Vazquez and Reid, 2004) and monazite (Williams et al., 1996), ThO^+/UO^+ RSF values for chevkinite range from 1.11 ± 0.03 to 1.29 ± 0.03 within single sessions, indicating preferential ionization of Th relative to U during sputtering of chevkinite. Measured $^{232}\text{Th}^{16}\text{O}^+/\text{U}^{16}\text{O}^+$ in multiple crystal fragments over several sessions yield a mean ratio of 18.0 ± 3.1 (1 s.d.). For zircon, Th/U relative sensitivity was determined using the observed $^{208}\text{Pb}^+/^{206}\text{Pb}^+/\text{U}^{16}\text{O}^+/\text{Th}^{16}\text{O}^+$ correlation of ca. 1.1 Ga AS3 zircon

standard (Reid et al., 1997; Schmitt, 2011). Reported $^{232}\text{Th}^{16}\text{O}^+/\text{U}^{16}\text{O}^+$ ratios for both chevkinite and zircon are adjusted with session-appropriate RSF values with propagation of uncertainty.

The $^{232}\text{Th}-^{230}\text{Th}-^{238}\text{U}-^{234}\text{U}$ isotope composition of La Primavera host rock samples were measured using a Nu multi-collector inductively-coupled mass spectrometer at University of California, Davis, following dissolution, chemical separation, and mass-spectrometry techniques described in Cooper and Donnelly (2008). The U–Th isotope composition of the West Yellowstone flow is reported in Vazquez and Reid (2002) and measured by thermal ionization mass spectrometry. The major and minor element compositions of Yellowstone chevkinite were measured using a JEOL 8200 electron microprobe at University of California, Los Angeles, and compositions of La Primavera chevkinite measured with a JEOL 8900 electron microprobe at USGS-Menlo Park. Analytical details, precisions, and detection limits of the electron microprobe analyses are provided in Appendix A.

3. Results

The U–Th isotope composition of La Primavera and Yellowstone chevkinite and zircon and their host rocks are listed in Tables 1 and 2, and representative compositions from electron microprobe measurements are listed in Table 3. Complete results from electron microprobe analyses are tabulated in Appendix A. All analyzed crystals yield $^{230}\text{Th}/^{238}\text{U}$ ratios indicating decay-chain disequilibrium, with $^{230}\text{Th}/^{238}\text{U}$ activity ratios of ~3 to ~6 (300 to 600% excesses). Individual chevkinite crystals analyzed with both SHRIMP-RG and CAMECA ion microprobes yield results that agree at the 95% confidence interval, despite sampling somewhat different intra-crystal domains after re-polishing of sample mounts between the analytical sessions (Table 1). Host rocks for La Primavera rhyolite yield ^{230}Th activity excesses of 10–12% relative to ^{238}U . Model ages for chevkinite and zircon from $^{238}\text{U}-^{230}\text{Th}$ disequilibrium are calculated as described in Reid et al. (1997), and range from ca. 50 ka to ca. 145 ka for La Primavera rhyolite, and ca. 115 ka to ca. 290 ka for Yellowstone rhyolite. Dates from chevkinite–zircon isochrons (Fig. 4) are calculated from error-weighted least-squares regression according to Mahon (1996). Reported uncertainties for isochron and mean model ages are expanded to account for scatter as represented by MSWD (mean square of weighted deviates; Wendt and Carl, 1991) and number of data as described by Ludwig and Titterington (1994). La Primavera and Yellowstone chevkinite crystals contain ThO_2 concentrations of ~0.5 to ~2.0 wt.% with Th/U between ~30 and ~50. Chevkinite from the pre- and post-caldera La Primavera rhyolites yield a restricted range of major and minor element compositions relative to those from the West Yellowstone flow.

4. Discussion

4.1. Crystallization ages from $^{238}\text{U}-^{230}\text{Th}$ dating of volcanic chevkinite

Dates derived from U–Th disequilibrium in chevkinite of typical microphenocryst size (>50 and <300 μm radius) in volcanic rocks will reflect crystallization if diffusion of U and Th is slow at the temperatures and timescales associated with magma chamber evolution. To date, experimental limits on U and Th diffusion in chevkinite are not established. An order-of-magnitude estimate of diffusion rate may be derived from the empirical relation between diffusivity and the ionic porosity of a mineral (Fortier and Giletti, 1989; Dahl, 1997). Ionic porosity is the proportion of a mineral's unit cell volume that is unoccupied by ions, with larger porosities being associated with higher rates of diffusion than for smaller porosities (Fortier and Giletti, 1989; Dahl, 1996, 1997). Following Dahl (1996) and Zhang (2008), an ionic porosity of 0.33 is calculated for chevkinite using observed compositions (Table 3), unit-cell data (Liziero, 2008), and effective ionic radii (Shannon, 1976). The relation between experimental diffusion parameters (Cherniak et al., 1997; Van Orman et al., 1998; Cherniak, 2005; Cherniak and Pyle, 2008) and

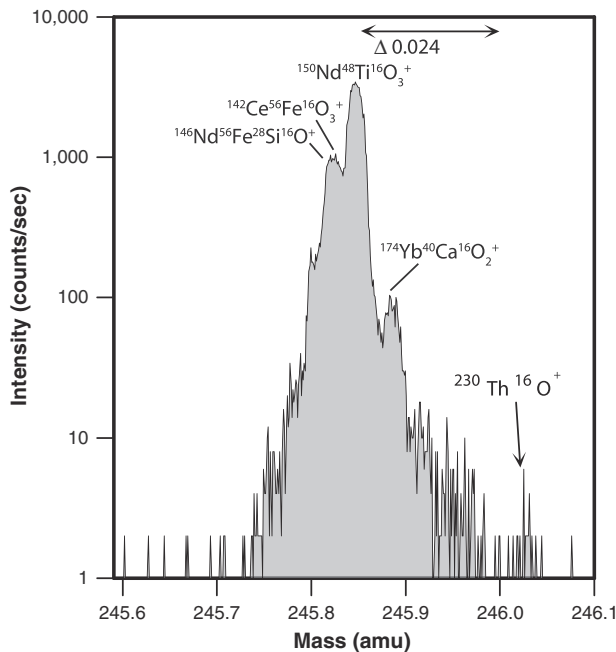


Fig. 3. Mass scan of $^{230}\text{Th}^{16}\text{O}^+$ region in Arondu chevkinite, with apparent molecular species and mass difference between NdTiO^+ guide peak and $^{230}\text{Th}^{16}\text{O}^+$ secondary ions. Distance between NdTiO⁺ guide peak and $^{230}\text{Th}^{16}\text{O}^+$ is 0.024 amu. Scan performed with SHRIMP-RG at mass resolution of ~8000.

Table 1

U-Th isotope data and model ages for La Primavera and West Yellowstone chevkinite.

Sample	Crystal #	$(^{238}\text{U})/(^{232}\text{Th})$	1 s.e.	$(^{230}\text{Th})/(^{232}\text{Th})$	1 s.e.	Model age (ka)	+ 1 σ	- 1 σ
<i>LP001 Rio Salado rhyolite (N 20° 40.704'; W 103° 34.711)</i>								
1270-LP001_LPC001B	1	0.0887	0.0022	0.517	0.023	111	8	7
RG-LP001-YCV09-12	1	0.0816	0.0016	0.449	0.027	135	12	11
RG-LP001-YCV09-13	1	0.0864	0.0017	0.447	0.029	137	13	12
1270-LP001_LPC002	2	0.0962	0.0026	0.556	0.024	100	8	7
RG-LP001-YCV09-17	2	0.0906	0.0018	0.535	0.032	106	11	10
1270-LP001_LPC003	3	0.0965	0.0025	0.579	0.023	94	7	6
1270-LP001_LPC004	4	0.0970	0.0024	0.553	0.024	101	8	7
RG-LP001-YCV09-8	4	0.0783	0.0016	0.438	0.026	138	12	10
RG-LP001-YCV09-9	4	0.0803	0.0016	0.422	0.027	146	13	12
1270-LP001_LPC005	5	0.0868	0.0023	0.560	0.025	98	8	7
RG-LP001-YCV-18	6	0.0813	0.0016	0.451	0.027	134	12	10
RG-LP001-YCV19	6	0.0859	0.0017	0.498	0.027	117	10	9
1270-LP001_LPC007	7	0.1113	0.0029	0.636	0.025	81	7	6
1270-LP001_LPC008	8	0.0949	0.0024	0.502	0.021	118	8	7
RG-LP001-YCV09-16	8	0.0830	0.0017	0.495	0.027	118	10	9
RG-LP001-YCV09-15	9	0.0849	0.0017	0.480	0.026	123	10	9
RG-LP001-YCV09-20	10	0.0847	0.0017	0.512	0.027	112	9	9
RG-LP001-YCV09-1	11	0.0782	0.0016	0.446	0.027	135	12	11
RG-LP001-YCV09-2	12	0.0904	0.0018	0.474	0.026	127	11	10
RG-LP001-YCV09-4	13	0.0855	0.0017	0.433	0.029	143	14	12
RG-LP001-YCV09-17d	14	0.0843	0.0017	0.452	0.028	134	12	11
<i>LP002B Rio Salado rhyolite (N 20° 40.763'; W 103° 34.776)</i>								
1270-LP002B-LPC-IM-001	1	0.0889	0.0035	0.438	0.025	141	12	11
1270-LP002B-LPC-IM-003	2	0.0914	0.0034	0.543	0.033	104	11	10
1270-LP002B-LPC-IM-005	3	0.0982	0.0039	0.504	0.039	118	15	13
1270-LP002B-LPC-IM-006	4	0.0952	0.0037	0.591	0.047	90	14	12
1270-LP002B-LPC-IM-007	5	0.0968	0.0037	0.443	0.033	142	16	14
1270-LP002B-LPC-IM-008	6	0.0867	0.0033	0.496	0.028	118	10	10
1270-LP002B-LPC-IM-012	7	0.0928	0.0035	0.594	0.056	89	16	14
1270-LP002B-LPC-IM-014	8	0.1132	0.0042	0.508	0.043	120	17	15
1270-LP002B-LPC-IM-015	9	0.0996	0.0038	0.556	0.033	101	11	10
LP002B whole rock		1.000	0.002	1.100	0.003			
<i>LP008 Arroyo Ixtahuatonte dome (N 20° 38.135'; W 103° 30.742)</i>								
1270-LP008-LPC-IM-001	1	0.1109	0.0044	0.724	0.070	56	16	14
1270-LP008-LPC-IM-004	2	0.0895	0.0033	0.526	0.048	106	17	15
1270-LP008-LPC001	3	0.1041	0.0021	0.622	0.037	79	10	9
1270-LP008-LPC002	4	0.0914	0.0019	0.597	0.031	84	9	8
1270-LP008-LPC004	5	0.0933	0.0019	0.754	0.032	48	7	6
LP008 whole rock		0.947	0.002	1.058	0.003			
<i>YCV-12 West Yellowstone flow (Vazquez and Reid, 2002)</i>								
RG-WY-CHV-1.1	1	0.1001	0.0019	0.431	0.016	116	11	10
RG-WY-CHV-3.1	3	0.0864	0.0016	0.293	0.012	206	17	15
RG-WY-CHV-3.2	3	0.0791	0.0015	0.292	0.011	200	15	13
RG-WY-CHV-4.1	4	0.1018	0.0019	0.313	0.014	198	21	17
RG-WY-CHV-7.1	7	0.0831	0.0016	0.315	0.012	182	14	13
RG-WY-CHV-7.2	7	0.0921	0.0017	0.346	0.014	163	14	13
RG-WY-CHV-9.1	9	0.0736	0.0014	0.255	0.010	240	21	17
RG-WY-CHV-10.1	10	0.0806	0.0015	0.257	0.010	247	22	18
RG-WY-CHV-12.1	12	0.0693	0.0013	0.228	0.009	279	26	21
RG-WY-CHV-13.1	13	0.0811	0.0015	0.327	0.011	170	12	11
RG-WY-CHV-2.1	14	0.0724	0.0014	0.227	0.009	289	28	22
YCV-09 whole rock ^a		0.745	0.001	0.852	0.003			

Analysis name contains prefix of 1270 or RG to denote measurement using CAMECA ims 1270 or SHRIMP-RG ion microprobes, respectively. Italicized analyses are excluded from isochron regressions. Decay constants used for activity ratios: $\lambda_{230} = 9.1705 \times 10^{-6} \text{ year}^{-1}$ (Cheng et al., 2013); $\lambda_{232} = 4.9475 \times 10^{-11} \text{ year}^{-1}$; $\lambda_{238} = 1.55125 \times 10^{-10} \text{ year}^{-1}$ (Jaffey et al., 1971; Steiger and Jäger, 1977). Model ages calculated using chevkinite-whole rock isochrons assuming secular equilibrium between ^{238}U and ^{234}U ; see text for details.

^a U-Th isotope analysis by thermal ionization mass spectrometry (Vazquez and Reid, 2002).

ionic porosity for various minerals (Dahl, 1996) suggests that diffusion rates for Th and U in chevkinite are on the orders of 10^{-27} and $10^{-28} \text{ m}^2/\text{s}$, respectively, at 850 °C. At these rates, a tabular chevkinite crystal with a 20 μm half-thickness would experience ≤ 0.6% fractional loss over the maximum timescale of 300 k.y. (Crank, 1975) that is resolvable by ion microprobe ^{238}U - ^{230}Th dating (cf. Reid et al., 1997). Monazite and allanite share similar ionic porosities (0.31–0.33; Dahl, 1997) to chevkinite, and yield ^{238}U - ^{206}Pb and ^{232}Th - ^{208}Pb ages that indicate retention of U and Th at the temperatures and timescales (10^5 – 10^6 yr) associated with silicic magmatism (e.g., Copeland et al., 1988; Oberli et al., 2004). Accordingly, chevkinite dates derived from ^{238}U - ^{230}Th disequilibrium are likely to reflect crystallization rather

than cooling. Dates derived from other elements that diffuse relatively quickly in chevkinite (e.g., He) yield cooling ages rather than crystallization ages (Min et al., 2006).

4.2. Isochron and model ages derived from chevkinite

Ages for the crystallization of accessory ± other minerals can be calculated from internal ^{238}U - ^{230}Th isochrons or using the Th-isotope composition of the host whole rock/glass as a model for the melt from which the crystals grew (Cooper and Reid, 2008; Schmitt, 2011). However, the relatively limited range of Th/U that appears characteristic of volcanic chevkinite in single samples effectively thwarts the derivation

Table 2

U-Th isotope data and model crystallization ages for La Primavera zircon.

Sample	(^{238}U)/(^{232}Th)	1 s.e.	(^{230}Th)/(^{232}Th)	1 s.e.	Model age (ka)	+1 σ	-1 σ	U (ppm)
<i>LP001 Rio Salado rhyolite</i>								
1270-LP001r3g003s1	4.71	0.13	3.43	0.08	108	9	9	985
1270-LP001-r3g004s1	5.39	0.15	3.97	0.07	116	9	8	1356
1270-LP001r3g008s1	5.20	0.12	3.76	0.10	109	9	9	176
1270-LP001r3g009s1	5.87	0.12	4.29	0.09	116	8	7	1345
1270-LP001r3g009s2	5.54	0.13	4.15	0.07	121	9	8	1084
1270-LP001r4g010s1	6.12	0.13	4.34	0.10	109	8	7	1442
1270-LP001r4g011s1	6.82	0.14	4.72	0.13	106	8	7	983
1270-LP001r4g014s1	5.14	0.14	3.68	0.07	106	8	8	721
1270-LP001r4g015s1	5.15	0.16	3.86	0.07	119	10	10	1328
1270-LP001r3g006s2	6.83	0.15	4.86	0.13	113	9	8	692
1270-LP001r4g007s1	6.74	0.16	5.01	0.11	125	10	9	1260
1270-LP001r2g002s1-1	5.66	0.12	4.28	0.09	125	9	9	1162
1270-LP001r2g013s1	5.63	0.12	4.46	0.11	141	13	11	1819
1270-LP001r2g005s1	3.72	0.15	2.98	0.08	128	18	16	1704
1270-LP001r4g007s1	6.74	0.16	5.01	0.11	125	10	9	1260
<i>LP002B Rio Salado rhyolite</i>								
1270-LPZ ZM 001	5.74	0.14	4.14	0.09	112	8	8	1795
1270-LPZ ZM 002	6.95	0.16	4.96	0.11	114	8	8	1312
1270-LPZ ZM 003	5.00	0.13	3.61	0.07	108	8	8	2285
1270-LPZ ZM 004	5.02	0.16	3.59	0.07	105	9	8	2483
1270-LPZ ZM 005	6.42	0.15	4.14	0.16	90	9	8	1223
1270-LPZ ZM 006	6.59	0.15	4.44	0.13	99	8	7	1266
1270-LPZ ZM 007	6.13	0.14	4.14	0.10	98	7	7	1552
1270-LPZ ZM 008	5.90	0.14	4.25	0.11	112	9	9	1581
<i>LP008 Arroyo Ixtahuatonte dome</i>								
1270-LPZ ZM 001	4.22	0.15	3.22	0.06	118	12	11	2824
1270-LPZ ZM 002	4.95	0.16	3.30	0.12	90	10	9	964
1270-LP Zr 001	5.51	0.33	3.48	0.32	83	20	17	671
1270-LP Zr 002	4.36	0.28	3.14	0.16	103	21	18	1312
1270-LP Zr 003	5.77	0.34	3.60	0.16	82	12	11	696
1270-LP Zr 004	5.51	0.33	3.56	0.15	87	13	12	953
1270-LP Zr 005	5.62	0.34	3.41	0.17	76	12	11	807

Uranium concentrations calculated from $\text{UO}_4^+/\text{Zr}_2\text{O}_4^+$ yields relative to 91,500 zircon (81.2 ppm U; Wiedenbeck et al., 1995). Decay constants used for activity ratios: $\lambda_{230} = 9.1705 \times 10^{-6} \text{ year}^{-1}$ (Cheng et al., 2013); $\lambda_{232} = 4.9475 \times 10^{-11} \text{ year}^{-1}$; $\lambda_{238} = 1.55125 \times 10^{-10} \text{ year}^{-1}$ (Jaffey et al., 1971; Steiger and Jäger, 1977). Model ages calculated using zircon-whole rock isochrons.

of precise internal isochrons (Fig. 4). This limited ability to generate internal isochrons also exists for volcanic allanite with its analogously high Th/U (e.g., Vazquez and Lidbarski, 2012), and contrasts with the typically variable Th/U of volcanic zircon. Accordingly, the derivation of precise isochron ages using chevkinite will almost always require one or more coeval phases with lower Th/U. Model ages for crystallization of individual chevkinite may be derived, but require an assumption

about initial Th-isotope composition during crystallization. In this study, initial Th-isotope composition is delimited by $^{238}\text{U}-^{230}\text{Th}-^{232}\text{Th}$ analyses of glassy whole rocks.

4.3. Timing of chevkinite crystallization in La Primavera and Yellowstone rhyolite

4.3.1. La Primavera chevkinite and zircon

The combined analyses of chevkinite in both samples of the Rio Salado rhyolite yield an uncertainty-weighted mean model age $117 \pm 7 \text{ ka}$ ($n = 30/30$, MSWD: 3.2, 95% confidence), or $121 \pm 6 \text{ ka}$ ($n = 26/30$, MSWD: 2.3, 95% confidence) if several apparent outliers are omitted. A chevkinite-zircon isochron (Fig. 4) for the Rio Salado rhyolite yields an age of $116 \pm 4 \text{ ka}$ ($n = 50/54$, MSWD: 2.0; 95% confidence). The whole rock compositions lie on this regression (Fig. 4), suggesting that chevkinite and zircon co-crystallized over the same brief interval. These ages are indistinguishable from the $124 \pm 4 \text{ ka}$ (2σ) K-Ar age for Rio Salado sanidine reported by Mahood and Drake (1982), suggesting that chevkinite and zircon crystallized just before the eruption of the pre-caldera rhyolite. Model ages for individual chevkinite from Arroyo Ixtahuatonte yield ages from ca. 50 ka to 105 ka, with a weighted mean of $71 \pm 31 \text{ ka}$ ($n = 5$, MSWD = 5.3, 95% confidence). The limited number ($n = 5$) of Arroyo Ixtahuatonte chevkinite is insufficient to generate a precise age, but combining chevkinite with coexisting zircon and whole rock yields an isochron age of $86 \pm 15 \text{ ka}$ ($n = 13$, MSWD = 4.2, 95% confidence), or $93 \pm 7 \text{ ka}$ ($n = 11/13$, MSWD = 1.5, 95% confidence) if two young outliers are excluded (Fig. 4). These ages for Arroyo Ixtahuatonte chevkinite and zircon are younger than those for Rio Salado, which is consistent with their relative positions in the volcanic stratigraphy, and are indistinguishable at the 95% confidence level

Table 3

Representative compositions of chevkinite from La Primavera (LP), Yellowstone (WY) rhyolite, and Pakistani pegmatite (Arondu).

Analys	LPC001B-2	LP008gr2-4	WY-CHV-1.1	WY-CHV-2.1	Arondu-Chip1-2
SiO ₂	20.45	19.88	20.44	21.14	18.95
TiO ₂	17.16	17.59	18.32	18.91	16.13
Al ₂ O ₃	0.26	0.27	0.56	0.71	0.32
FeO	10.92	11.49	10.79	10.42	12.30
MnO	0.25	0.25	0.07	0.07	0.50
MgO	0.02	0.03	0.23	0.37	0.29
CaO	2.79	2.91	2.90	3.06	2.37
ThO ₂	0.88	0.57	1.30	1.27	1.67
La ₂ O ₃	12.09	13.18	11.37	11.53	11.24
Ce ₂ O ₃	21.90	22.76	21.17	21.26	22.76
Pr ₂ O ₃	1.84	1.68	2.16	2.25	2.09
Nd ₂ O ₃	7.33	6.80	7.65	7.67	7.91
Sm ₂ O ₃	0.86	0.60	0.96	0.85	0.68
Gd ₂ O ₃	0.55	0.36	0.68	0.64	0.22
Y ₂ O ₃	0.51	0.32	0.66	0.68	0.01
ZrO ₂	0.46	0.65	0.53	0.32	0.13
Nb ₂ O ₅	0.94	0.58	1.01	0.66	0.30
Total	99.19	99.94	99.28	100.82	97.88

Concentrations determined via electron microprobe. Analytical details provided in Appendix A.

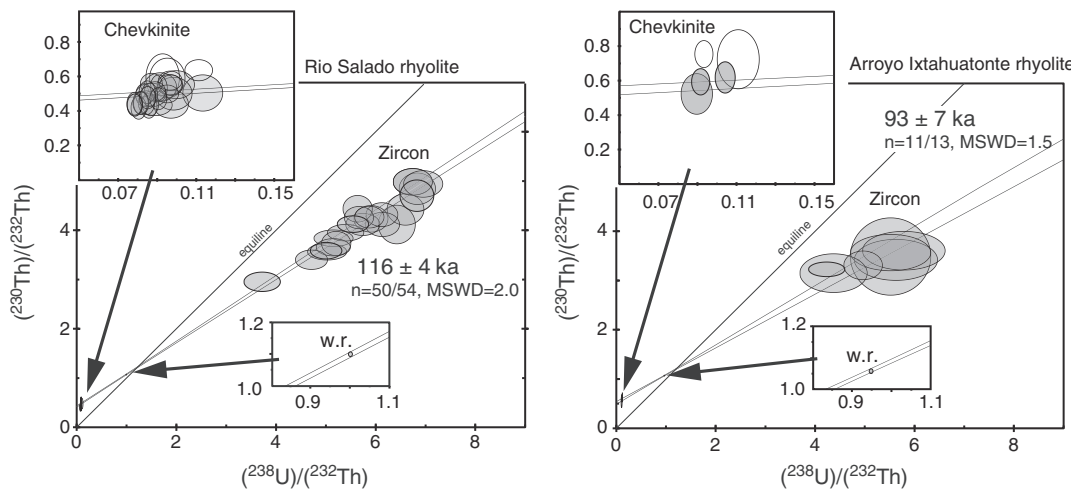


Fig. 4. Isochron diagrams with ^{238}U - ^{230}Th - ^{232}Th (activity) compositions of chevkinite and zircon from La Primavera rhyolite. Ellipses represent 2σ analytical uncertainties. Open ellipses are data excluded from isochron calculation (Table 1). Calculated dates are given at the 95% confidence level.

from the 84 ± 4 ka (2σ) K-Ar age for coexisting sanidine (Mahood and Drake, 1982).

The highly evolved nature and isotopic compositions of La Primavera rhyolites suggest derivation via extensive fractional crystallization of mantle-derived magma and/or melting of lower crustal mafic rocks (Mahood and Halliday, 1988). Highly evolved rhyolites that are crystal-poor, such as those erupted from La Primavera and Yellowstone calderas, are often attributed to fractionation of crystal-poor magma from a crystal-rich reservoir of magma "mush" (e.g., Hildreth, 2004; Macdonald, 2012). The indistinguishable U-Th and K-Ar ages for both Rio Salado and Arroyo Ixtahuatonte rhyolites suggest a geologically brief interval of crystallization prior to eruption, and in turn relatively short residence of eruptible magma following its fractionation from a crystal-rich parent. Alternatively, crystallization may have occurred after an episode of magma heating that fully resorbed preexisting chevkinite and zircon, although there is no apparent geochemical or petrographic evidence for heating or magma mixing. Zircon saturation temperatures (Boehnke et al., 2013) based on bulk rhyolite composition and reported Zr concentrations (Mahood, 1981) are 840°C and 860°C for Rio Salado and Arroyo Ixtahuatonte rhyolites, respectively, which effectively match an apparent eruption temperature of $\sim 850^\circ\text{C}$ from Fe-Ti oxides (Mahood, 1981). These near-identical zircon saturation and eruption temperatures are consistent with the dating results indicating a geologically short interval for chevkinite + zircon crystallization prior to eruption.

4.3.2. West Yellowstone flow chevkinite and zircon

Chevkinite crystals from the West Yellowstone flow yield model crystallization ages ranging from ca. 115 ka to ca. 290 ka (Table 1; Fig. 5). This range of ages matches the range of model crystallization ages for zircon from the same hand sample (Fig. 5). Vazquez and Reid (2002) interpreted this range of zircon ages to reflect the protracted cooling and crystallization to near-solidus conditions at ca. 120 ka in the voluminous magma reservoir that fed the CPM rhyolites, with ages greater than ca. 200 ka likely representing antecrysts or inherited domains. The overlapping intervals of crystallization for chevkinite and zircon suggest persistence of the thermochemical conditions required for saturation of both minerals in post-caldera rhyolite at Yellowstone. Zircon saturation temperatures for the West Yellowstone flow rhyolite are $\sim 800^\circ\text{C}$ based on the model of Boehnke et al. (2013), with pyroxene-fayalite and Fe-Ti oxide phenocryst compositions yielding temperatures of $845\text{--}860^\circ\text{C}$ (Vazquez et al., 2009). Only the youngest chevkinite model age overlaps the 114 ± 2 ka eruption age derived by $^{40}\text{Ar}/^{39}\text{Ar}$ dating of sanidine (Christiansen et al., 2007). Dating of near-eruption growth on the chevkinite crystals is likely to require ion microprobe sampling of unpolished rim surfaces of individual crystals

in the same manner that has been used for other accessory minerals (e.g., Schmitt et al., 2011; Vazquez and Lidzbarski, 2012).

4.4. Age-compositional relations of La Primavera and Yellowstone chevkinite

Differentiation of metaluminous silicic magma and/or increasing peralkalinity typically results in crystallization of chevkinite with higher La, Ce, Mn, Fe, and Nb concentrations, and lower Al, Ti, Mg, Ca, and MREE concentrations (Macdonald et al., 2002, 2009). The compositions of La

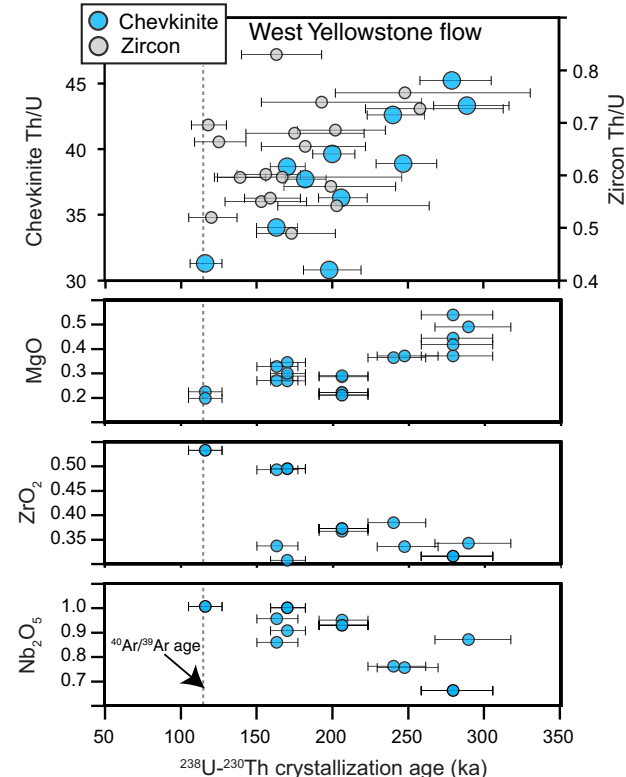


Fig. 5. Th/U versus ^{238}U - ^{230}Th model crystallization age for West Yellowstone flow chevkinite (blue circles) and zircon (gray circles). Zircon data are from Vazquez and Reid (2002) with ages recalculated using ^{230}Th decay constant of Cheng et al. (2013). Concentrations of Nb, Zr, and Mg in West Yellowstone chevkinite are from electron microprobe analyses and are correlated to their respective U-Th age. $^{40}\text{Ar}/^{39}\text{Ar}$ eruption age of ca. 115 ka (Christiansen et al., 2007) is denoted by vertical dashed line.

Primavera and Yellowstone chevkinite follow this general trend and are consistent with increasing magnitude of differentiation and/or peralkalinity of their host rocks. West Yellowstone chevkinite has lower average Th/U, Mg/Fe, Fe and Th, and higher average Mn, Zr, and Nb with decreasing age (Fig. 5). These trends mimic the general trend of groundmass glass compositions for rhyolites erupted over the same ca. 115 ka–260 ka interval (Vazquez et al., 2009), as well as a general decrease in Th/U between the interiors and rims of West Yellowstone zircon from the same sample (Fig. 5). The most evolved, i.e., lowest Mg, chevkinite crystals from the West Yellowstone flow are similar in composition to those occurring in the ca. 640 ka Lava Creek Tuff (Fig. 6), but they are 100's of k.y. younger.

The La Primavera pre-caldera Rio Salado and post-caldera Arroyo Ixtahuatonte chevkinite appear to lie along the same general compositional trend defined by the West Yellowstone rhyolite, with some overlap in compositions (Fig. 6). Based on major element chemistry, the weakly peralkaline host rhyolites from La Primavera are broadly comparable to those of West Yellowstone, but based on trace elements, La Primavera rhyolites are even more evolved ($\text{Rb}/\text{Sr} = 100\text{--}250$ and $[\text{Sr}] = 0.5\text{--}1.5 \text{ ppm}$) than post-caldera rhyolites at Yellowstone ($\text{Rb}/\text{Sr} = 2\text{--}140$ and $[\text{Sr}] = 2\text{--}85 \text{ ppm}$) (Mahood and Halliday, 1988; Halliday et al., 1991; Vazquez and Reid, 2002). Rio Salado and Arroyo Ixtahuatonte rhyolites are nearly identical in bulk and trace element composition, reflecting compositional rebound of the La Primavera magmatic system in the ca. 95–85 ka interval after the caldera-forming eruption of the compositionally zoned Tala Tuff magma (Mahood, 1981). Rio

Salado rhyolite primarily differs from Arroyo Ixtahuatonte rhyolite by having higher Rb, Y, and U, lower Zr concentrations, and slightly lower peralkalinity (Mahood, 1981). Chevkinite in both rhyolites mirrors the overall similarities and distinctions in terms of major and trace element concentrations between the whole rocks, with lower Zr and La, and higher Y in chevkinite from the older Rio Salado rhyolite. Concentrations of Nb are significantly different between the Rio Salado and Arroyo Ixtahuatonte chevkinite, but their relative Zr/Nb is consistent with that for the two rhyolites (cf. Mahood, 1981). These geochemical characteristics are consistent with reorganization and renewed differentiation of the subcaldera magma reservoir by addition of new rhyolite from deeper levels in the magmatic system immediately after evacuation of the Tala Tuff magma chamber (Mahood, 1981).

5. Summary and conclusions

High Th concentrations and large magnitude Th/U fractionation during crystallization from rhyolitic magma make volcanic chevkinite amenable to $^{230}\text{Th}/^{238}\text{U}$ disequilibrium dating via secondary ion mass spectrometry. Ion microprobe measurements of chevkinite microphenocrysts from rhyolite lavas erupted before and after formation of La Primavera caldera yield U–Th crystallization ages that are similar to their respective sanidine K–Ar ages of ca. 125 ka and ca. 85 ka, indicating a geologically brief interval between magma crystallization and volcanic eruption. Chevkinite from post-caldera rhyolite at Yellowstone caldera yield U–Th dates between ca. 115 ka and ca. 300 ka, which matches the range of crystallization ages from coexisting zircon. The typically restricted range in Th/U for related volcanic chevkinite thwarts the generation of precise chevkinite-only isochrons, but combination with zircon and/or major phases with relatively low Th/U can produce mid- to late-Pleistocene isochron dates with precision of ~5%. The major and minor element compositions of chevkinite from La Primavera and Yellowstone rhyolites are consistent with the relative degrees of differentiation and/or peralkalinity of their host magmas, and can be keyed to their respective U–Th crystallization ages to resolve the age-compositional evolution of rhyolitic magma.

Acknowledgments

The U.S. Geological Survey and National Science Foundation award GEO-0503609 supported this research. The ion microprobe facility at UCLA is partly supported by a grant from the Instrumentation and Facilities Program, Division of Earth Sciences, National Science Foundation. We are grateful to Cristo Ramirez for the assistance during sample collection at La Primavera. We thank Brad Ito, George Jarzebinski, Frank Kyte, and Robert Oscarson for their technical assistance and instrument maintenance, and also Andy Calvert, Calvin Miller, and Anonymous for their manuscript reviews.

Appendix A. Supplementary data

Supplementary data to this article can be found online at <http://dx.doi.org/10.1016/j.chemgeo.2014.10.020>.

References

- Bacon, C.R., 1989. Crystallization of accessory phases in magmas by local saturation adjacent to phenocrysts. *Geochim. Cosmochim. Acta* 53, 1055–1066.
- Bacon, C., Lowenstern, J., 2005. Late Pleistocene granodiorite source for recycled zircon and phenocrysts in rhyodacite lava at Crater Lake, Oregon. *Earth Planet. Sci. Lett.* 233, 277–293.
- Bacon, C.R., Sisson, T.W., Mazdab, F.K., 2007. Young cumulate complex beneath Veniaminof caldera, Aleutian arc, dated by zircon in erupted plutonic blocks. *Geology* 35, 491–494.
- Boehnke, P., Watson, E.B., Trail, D., Harrison, T.M., Schmitt, A.K., 2013. Zircon saturation revisited. *Chem. Geol.* 351, 324–334. <http://dx.doi.org/10.1016/j.chemgeo.2013.05.028>.
- Cameron, K., Cameron, M., 1986. Whole-rock/groundmass differentiation trends of rare earth elements in high-silica rhyolites. *Geochim. Cosmochim. Acta* 50, 759–769.

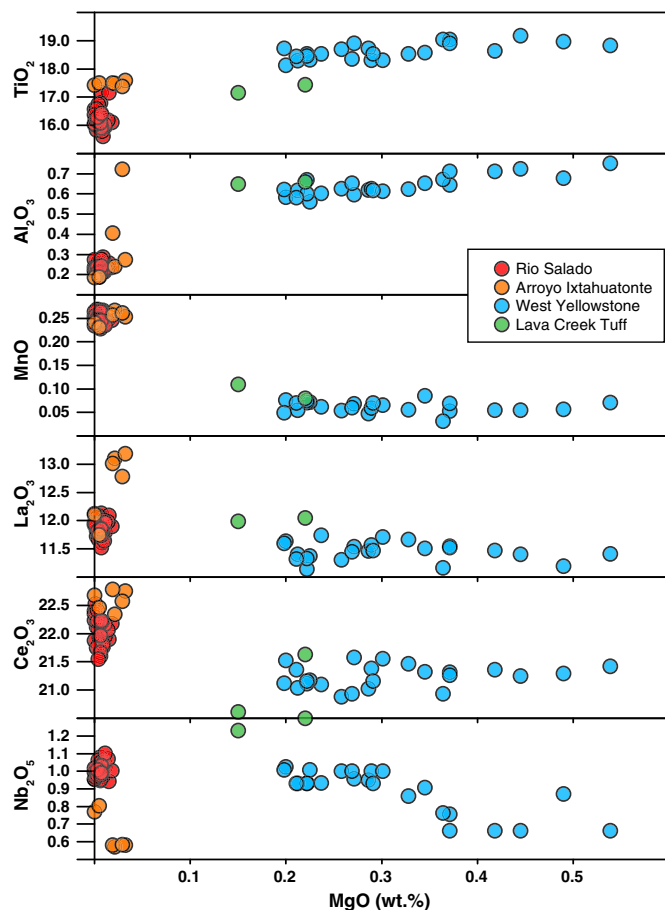


Fig. 6. Compositions of chevkinite from Rio Salado (red circles), Arroyo Ixtahuatonte (orange circles), and West Yellowstone rhyolites (blue circles) from electron microprobe analyses. Lava Creek Tuff chevkinite reported by Macdonald and Belkin (2002) is shown as blue circles. Increasing Ce, La, Nb and Mn, and decreasing Al, and Ti relative to Mg in chevkinite are consistent with crystallization from melts that are more evolved and/or more peralkaline (Macdonald and Belkin, 2002).

- Cheng, H., Edwards, R.L., Shen, C.-C., Polyak, V.J., Asmerom, Y., Woodhead, J., Hellstrom, J., Wang, Y., Kong, X., Spötl, C., Wang, X., Alexander, E.C., 2013. Improvements in ^{230}Th dating, ^{230}Th and ^{234}U half-life values, and U-Th isotopic measurements by multi-collector inductively coupled plasma mass spectrometry. *Earth Planet. Sci. Lett.* 371–372, 82–91. <http://dx.doi.org/10.1016/j.epsl.2013.04.006>.
- Cherniak, D.J., 2005. Uranium and manganese diffusion in apatite. *Chem. Geol.* 219, 297–308.
- Cherniak, D.J., Pyle, J.M., 2008. Thorium diffusion in monazite. *Chem. Geol.* 256, 52–61.
- Cherniak, D.J., Hanchar, J.M., Watson, E.B., 1997. Diffusion of tetravalent cations in zircon. *Contrib. Mineral. Petro.* 127, 383–390.
- Christiansen, R.L., 2001. The Quaternary and Pliocene Yellowstone Plateau volcanic field of Wyoming, Idaho, and Montana. US Geol. Surv. Prof. Pap. 729-G (145 p.).
- Christiansen, R., Blank, H., 1972. Volcanic stratigraphy of the Quaternary Plateau Rhyolite. US Geol. Surv. Prof. Pap. 729-B, 18.
- Christiansen, R.L., Lowenstern, J., Smith, R., Heasler, H., Morgan, L., Nathenson, M., Mastin, L., Muffler, L., Robinson, J., 2007. Preliminary assessment of volcanic and hydrothermal hazards in Yellowstone National Park and vicinity. US Geol. Surv. Open-File Rep. 2007-1071 98 p.
- Cooper, K.M., Donnelly, C.T., 2008. ^{238}U - ^{230}Th - ^{226}Ra disequilibrium in dacite and plagioclase from the 2004–2005 eruption of Mount St. Helens. US Geol. Surv. Prof. Pap. 1750, 827–846.
- Cooper, K., Reid, M., 2008. Uranium-series crystal ages. *Rev. Mineral. Geochem.* 69, 479–544.
- Copeland, P., Parrish, R.R., Harrison, T.M., 1988. Identification of inherited radiogenic Pb in monazite and its implications for U-Pb systematics. *Nature* 333, 760–763. <http://dx.doi.org/10.1038/333760a0>.
- Costa, F., 2008. Residence times of silicic magmas associated with calderas. *Dev. Volcanol.* 10, 1–55.
- Crank, J., 1975. The Mathematics of Diffusion. Oxford Science Publications, (414 p.).
- Cubukcu, H., Aydar, E., Gourgaud, A., 2007. Comment on “volcanostratigraphy and petrogenesis of the Nemrut stratovolcano (East Anatolian High Plateau): the most recent post-collisional volcanism in Turkey” by Özdemir et al. [Chemical Geology 226 (2006) 189–211]. *Chem. Geol.* 245, 120–129. <http://dx.doi.org/10.1016/j.chemgeo.2007.07.012>.
- Dahl, P.S., 1996. The effects of composition on retentivity of argon and oxygen in hornblende and related amphiboles: a field-tested empirical model. *Geochim. Cosmochim. Acta* 60, 3687–3700.
- Dahl, P.S., 1997. A crystal-chemical basis for Pb retention and fission-track annealing systematics in U-bearing minerals, with implications for geochronology. *Earth Planet. Sci. Lett.* 150, 277–290.
- Fortier, S.M., Giletti, B., 1989. An empirical model for predicting diffusion coefficients in silicate minerals. *Science* 245, 1481–1484.
- Fukuoka, T., Kigoshi, K., 1974. Discordant I_{O} ages and the uranium and thorium distribution between zircon and hosts rocks. *Geochim. J.* 8, 117–122.
- Gelman, S.E., Gutierrez, F.J., Bachmann, O., 2013. On the longevity of large upper crustal magma reservoirs. *Geology* 41, 759–762.
- Green, T.H., Pearson, N.J., 1988. Experimental crystallization of chevkinite/perrierite from REE-enriched silicate liquids at high pressure and temperature. *Mineral. Mag.* 52, 113–120.
- Halliday, A.N., Davidson, J.P., Hildreth, W., Holden, P., 1991. Modelling the petrogenesis of high Rb/Sr silicic magmas. *Chem. Geol.* 92, 107–114.
- Heumann, A., Davies, G.R., 2002. U-Th disequilibrium and Rb-Sr age constraints on the magmatic evolution of peralkaline rhyolites from Kenya. *J. Petrol.* 43, 557–577.
- Hildreth, W., 2004. Volcanological perspectives on Long Valley, Mammoth Mountain, and Mono Craters: several contiguous but discrete systems. *J. Volcanol. Geotherm. Res.* 136, 169–198.
- Hildreth, W., Christiansen, R.L., O’Neil, J.R., 1984. Catastrophic isotopic modification of rhyolitic magma at times of caldera subsidence: Yellowstone Plateau volcanic field. *J. Geophys. Res.* 89, 8339–8369.
- Izett, G.A., Wilcox, R.E., 1968. Perrierite, chevkinite, and allanite in upper Cenozoic ash beds in the Western United States. *Am. Mineral.* 53, 1558–1567.
- Jaffey, A.H., Flynn, K.F., Glendenin, L., Bentley, W.C., Essling, A.M., 1971. Precision measurement of half-lives and specific activities of ^{235}U and ^{238}U . *Phys. Rev. C* 4, 1889–1906.
- Johnson, C., Czamanske, G., Lipman, P., 1989. Geochemistry of intrusive rocks associated with the Latir volcanic field, New Mexico, and contrasts between evolution of plutonic and volcanic rocks. *Contrib. Mineral. Petro.* 103, 90–109.
- Lanphere, M.A., Champion, D.E., Christiansen, R.L., Izett, G.A., Obradovich, J.D., 2002. Revised ages for tufts of the Yellowstone Plateau volcanic field: assignment of the Huckleberry Ridge Tuff to a new geomagnetic polarity event. *Geol. Soc. Am. Bull.* 114, 559–568.
- Liziero, F., 2008. Studio Cristallochimico E Strutturale Di Chevkiniti-(Ce) Non MetamittichePhD Dissertation Universita' Degli Studi Di Padova, pp. 1–129.
- Lowenstern, J., Clyne, M., Bulen, T., 1997. Comagmatic A-type granophyre and rhyolite from the Alid volcanic center, Eritrea, northeast Africa. *J. Petrol.* 38, 1707–1721.
- Ludwig, K.R., Titterington, D.M., 1994. Calculation of $^{230}\text{Th}/\text{U}$ isochrons, ages, and errors. *Geochim. Cosmochim. Acta* 58, 5031–5042.
- Macdonald, R., 2012. Evolution of peralkaline silicic complexes: lessons from the extrusive rocks. *Lithos* 152, 11–22.
- Macdonald, R., Belkin, H.E., 2002. Compositional variation in minerals of the chevkinite group. *Mineral. Mag.* 66, 1075–1098.
- Macdonald, R., Marshall, A.S., Dawson, J.B., Hinton, R.W., Hill, P.G., 2002. Chevkinite-group minerals from salic volcanic rocks of the East Africa Rift. *Mineral. Mag.* 66, 287–299.
- Macdonald, R., Belkin, H., Wall, F., Baginski, B., 2009. Compositional variation in the chevkinite group: new data from igneous and metamorphic rocks. *Mineral. Mag.* 73, 777–796.
- Mahon, K.L., 1996. The New “York” regression: application of an improved statistical method to geochemistry. *Int. Geol. Rev.* 38, 293–303.
- Mahood, G.A., 1980. Geological evolution of a Pleistocene rhyolitic center-Sierra La Primavera, Jalisco, México. *J. Volcanol. Geotherm. Res.* 8, 199–230.
- Mahood, G.A., 1981. Chemical evolution of a Pleistocene rhyolitic center: Sierra La Primavera, Jalisco, México. *Contrib. Mineral. Petro.* 77, 129–149.
- Mahood, G.A., Drake, R.E., 1982. K-Ar dating young rhyolitic rocks: a case study of the Sierra La Primavera, Jalisco, Mexico. *Geol. Soc. Am. Bull.* 93, 1232–1241.
- Mahood, G.A., Halliday, A.N., 1988. Generation of high-silica rhyolite: a Nd, Sr, and O isotopic study of Sierra La Primavera, Mexican Neovolcanic Belt. *Contrib. Mineral. Petro.* 100, 182–191.
- McDowell, S.D., 1979. Chevkinite from the Little Chief Granite, porphyry stock, California. *Am. Mineral.* 64, 721–727.
- Michael, P.J., 1988. Partition coefficients for rare earth elements in mafic minerals of high silica rhyolites: the importance of accessory mineral inclusions. *Geochim. Cosmochim. Acta* 52, 275–282.
- Mills Jr., J.G., Saltoun, B.W., Vogel, T.A., 1997. Magma batches in the Timber Mountain magmatic system, southwestern Nevada volcanic field, Nevada, USA. *J. Volcanol. Geotherm. Res.* 78, 185–208.
- Min, K., Reiners, P., Wolff, J., Mundil, R., Winters, R., 2006. (U-Th)/He dating of volcanic phenocrysts with high-U-Th inclusions, Jemez Volcanic Field, New Mexico. *Chem. Geol.* 227, 223–235.
- Novak, S.W., Mahood, G.A., 1986. Rise and fall of a basalt-trachyte-rhyolite magma system at the Kain Springs Wash Caldera, Nevada. *Contrib. Mineral. Petro.* 94, 352–373. <http://dx.doi.org/10.1007/BF00371444>.
- Oberli, F., Meier, M., Berger, A., Rosenberg, C.L., Giere, R., 2004. U-Th-Pb and $^{230}\text{Th}/^{238}\text{U}$ disequilibrium isotope systematics: precise accessory mineral chronology and melt evolution tracing in the Alpine Bergell intrusion. *Geochim. Cosmochim. Acta* 68, 2543–2560.
- Parker, D.F., White, J.C., 2007. Large-scale silicic alkalic magmatism associated with the Buckhorn Caldera, Trans-Pecos Texas, USA: comparison with Pantelleria, Italy. *Bull. Volcanol.* 70, 403–415. <http://dx.doi.org/10.1007/s00445-007-0145-2>.
- Pyle, D.M., Ivanovich, M., Sparks, R.S.J., 1988. Magma-cumulate mixing identified by U-Th disequilibrium dating. *Nature* 331, 157–159.
- Reid, M.R., Coath, C.D., Harrison, T.M., McKeegan, K.D., 1997. Prolonged residence times for the youngest rhyolites associated with Long Valley Caldera: $^{230}\text{Th}-^{238}\text{U}$ ion microprobe dating of young zircons. *Earth Planet. Sci. Lett.* 150, 27–39.
- Ridolfi, F., Renzulli, A., Santi, P., Upton, B., 2003. Evolutionary stages of crystallization of weakly peralkaline syenites: evidence from ejecta in the plinian deposits of Agua de Pau volcano (Sao Miguel, Azores Islands). *Mineral. Mag.* 67, 749–767.
- Robinson, D., Miller, C., 1999. Record of magma chamber processes preserved in accessory mineral assemblages, Aztec Wash Pluton, Nevada. *Am. Mineral.* 84, 1346–1353.
- Scaillet, B., Macdonald, R., 2001. Phase relations of peralkaline silicic magmas and petrogenetic implications. *J. Petrol.* 42, 825–845.
- Scaillet, B., Macdonald, R., 2003. Experimental constraints on the relationships between peralkaline rhyolites of the Kenya Rift Valley. *J. Petrol.* 44, 1867–1894.
- Schmitt, A.K., 2011. Uranium series accessory crystal dating of magmatic processes. *Annu. Rev. Earth Planet. Sci.* 39, 321–349. <http://dx.doi.org/10.1146/annurev-earth-040610-133330>.
- Schmitt, A.K., Emmermann, R., Trumbull, R.B., Bühn, B., Henjes-Kunst, F., 2000. Petrogenesis and $^{40}\text{Ar}/^{39}\text{Ar}$ geochronology of the Brandberg Complex, Namibia: evidence for a major mantle contribution in metaluminous and peralkaline granites. *J. Petrol.* 41, 1207–1239.
- Schmitt, A.K., Stockli, D.E., Hausback, B.P., 2006. Eruption and magma crystallization ages of Las Tres Virgenes (Baja California) constrained by combined $^{230}\text{Th}/^{238}\text{U}$ and (U-Th)/He dating of zircon. *J. Volcanol. Geotherm. Res.* 158, 281–295.
- Schmitt, A.K., Danišík, M., Evans, N.J., Siebel, W., Kiemele, E., Aydin, F., Harvey, J.C., 2011. Acıgöl rhyolite field, Central Anatolia (part 1): high-resolution dating of eruption episodes and zircon growth rates. *Contrib. Mineral. Petro.* 162, 1–17.
- Shannon, R.D., 1976. Revised effective ionic radii and systematic studies of interatomic distances in halides and chalcogenides. *Acta Crystallogr. A32*, 751–767.
- Steiger, R., Jäger, E., 1977. Subcommission on geochronology: convention on the use of decay constants in geo-and cosmochronology. *Earth Planet. Sci. Lett.* 36, 359–362.
- Stelten, M.E., Cooper, K.M., Vazquez, J.A., Reid, M.R., Barfond, G.H., Wimpenny, J., Yin, Q.-Z., 2013. Magma mixing and generation of isotopically juvenile silicic magma at Yellowstone caldera inferred from coupling ^{238}U - ^{230}Th age with trace elements and Hf and O isotopes in zircon and Pb isotopes in sanidine. *Contrib. Mineral. Petro.* 166, 587–613. <http://dx.doi.org/10.1007/s00410-013-0893-2>.
- Storm, S., Shane, P., Schmitt, A.K., Lindsay, J.M., 2011. Decoupled crystallization and eruption histories of the rhyolite magmatic system at Tarawera volcano revealed by zircon ages and growth rates. *Contrib. Mineral. Petro.* 163, 505–519. <http://dx.doi.org/10.1007/s00410-011-0682-8>.
- Troll, V.R., Sachs, P.M., Schmincke, H.U., Sumita, M., 2003. The REE-Ti mineral chevkinite in comenditic magmas from Gran Canaria, Spain: a SYXRF-probe study. *Contrib. Mineral. Petro.* 145, 730–741.
- Van Orman, J.A., Grove, T.L., Shimizu, N., 1998. Uranium and thorium diffusion in diopside. *Earth Planet. Sci. Lett.* 160, 505–519.
- Vazquez, J.A., Lidzbarski, M.I., 2012. High-resolution tephrochronology of the Wilson Creek Formation (Mono Lake, California) and Laschamp event using $^{238}\text{U}/^{230}\text{Th}$ SIMS dating of accessory mineral rims. *Earth Planet. Sci. Lett.* 357–358, 54–67. <http://dx.doi.org/10.1016/j.epsl.2012.09.013>.
- Vazquez, J.A., Reid, M.R., 2002. Time scales of magma storage and differentiation of voluminous high-silica rhyolites at Yellowstone caldera, Wyoming. *Contrib. Mineral. Petro.* 144, 274–285.
- Vazquez, J.A., Reid, M.R., 2004. Probing the accumulation history of the voluminous Toba magma. *Science* 305, 991–994.
- Vazquez, J.A., Kyriazis, S.F., Reid, M.R., Sehler, R.C., Ramos, F.C., 2009. Thermochemical evolution of young rhyolites at Yellowstone: evidence for a cooling but periodically replenished postcaldera magma reservoir. *J. Volcanol. Geotherm. Res.* 188, 186–196.

- Verplanck, P., Farmer, G., McCurry, M., Mertzman, S.A., 1999. The chemical and isotopic differentiation of an epizonal magma body: Organ Needle Pluton, New Mexico. *J. Petrol.* 40, 653–678.
- Vlach, S.R.F., Gualda, G.A.R., 2007. Allanite and chevkinite in A-type granites and syenites of the Graciosa Province, southern Brazil. *Lithos* 97, 98–121.
- Walker, G.P.L., Wright, J.P., Clough, B.J., Booth, B., 1981. Pyroclastic geology of the rhyolitic volcano of La Primavera, Mexico. *Int. J. Earth Sci.* 70 (3), 1100–1118.
- Watts, K.E., Bindeman, I.N., Schmitt, A.K., 2012. Crystal scale anatomy of a dying supervolcano: an isotope and geochronology study of individual phenocrysts from voluminous rhyolites of the Yellowstone caldera. *Contrib. Mineral. Petrol.* 164, 45–67. <http://dx.doi.org/10.1007/s00410-012-0724-x>.
- Wendt, I., Carl, C., 1991. The statistical distribution of the mean squared weighted deviation. *Chem. Geol.* 86, 275–285.
- Wetzel, F., Schmitt, A.K., Kronz, A., Wörner, G., 2010. In situ ^{238}U – ^{230}Th disequilibrium dating of pyrochlore at sub-millennial precision. *Am. Mineral.* 95, 1353–1356.
- Wiedenbeck, M., Alle, P., Corfu, F., Griffin, W.L., Meier, M., Oberli, F., von Quadt, A., Roddick, J.C., Spiegel, W., 1995. Three natural zircon standards for U-Th-Pb, Lu-Hf, trace element and REE analyses. *Geostandards Newsletter* 19, 1–23.
- Williams, I.S., Buick, I.S., Cartwright, I., 1996. An extended episode of early Mesoproterozoic metamorphic fluid flow in the Reynolds Range, central Australia. *J. Metamorph. Geol.* 14, 29–47. <http://dx.doi.org/10.1111/j.1525-1314.1996.00029.x>.
- Young, E.J., Powers, H.A., 1960. Chevkinite in volcanic ash. *Am. Mineral.* 45, 875–881.
- Zhang, Y., 2008. *Geochemical Kinetics*. Princeton University Press, Princeton New Jersey.